

# Extremely slow scaling of minimal Hamming distance in quantum sampling data

P. S. Golubev,<sup>1</sup> I. A. Iakovlev,<sup>1,2</sup> and V. V. Mazurenko<sup>1,2</sup>

<sup>1</sup>*Theoretical Physics and Applied Mathematics Department,  
Ural Federal University, Ekaterinburg 620002, Russia*

<sup>2</sup>*Russian Quantum Center, Skolkovo, Moscow 121205, Russia*

Quantum data can be obtained from a diverse range of sources, including direct measurements from noisy quantum processors, cold-atom simulators, and classical approximations such as variational neural-network states. However, our ability to characterize these systems is fundamentally limited, as the available measurement data is often sparse compared to the exponentially large Hilbert space of the system. To address this, we propose using the average minimal Hamming distance calculated for a set of unique bitstrings as a robust metric revealing a universal power-law behaviour. Through various examples of real experiments and simulations, we show that the power-law parameters reliably capture the complexity of quantum states and identify quantum phase transitions from limited quantum information, without the need for accumulating extensive statistics or explicitly calculating physical observables. This enables the analysis of completely different quantum experiments within a single framework.

Quantum state measurement is an integral part of any quantum experiment, including quantum computing, where the final wave function encodes a solution of a problem. The resulting basis states, represented as bitstrings (for instance, '01000..1', '11010..1'), provide only limited information regarding the underlying quantum state, as they are typically few in number compared to the dimensionality of the Hilbert space. This makes extracting the maximum amount of useful information from quantum measurements a nontrivial problem that lacks a universal solution. Numerous measurement-based approaches for characterizing quantum states developed to date mainly focus on estimating standard inter-qubit correlation functions and entropies of different types [1–5]. Alternative approaches [6–10] treat bit-string arrays as datasets, revealing patterns and quantifying correlations between different samples, effectively abstracting away the quantum origin of the input. Here, various metrics from data science can be applied, and subsequently leveraged as hash functions for the underlying quantum states, facilitating their efficient certification.

A primary procedure in processing bit-string arrays for some high-level algorithms mentioned above is the calculation of the Hamming distance [11], which quantifies the number of bits by which two samples differ. For instance, within the wave-function network approaches [12–16] the minimal Hamming distance averaged over a bit-string array determines the structure of the graph subsequently used for analysis of the quantum state. In certain situations, the Hamming distance on its own facilitates the solution of a problem where error correction [17] and discrimination of non-trivial non-equilibrium quantum states [18, 19] serve as prominent examples. While the Hamming distance metric is extensively applied in quantum computing, its behavior is still poorly understood.

In this work, we characterize state spaces of notable quantum states at the level of projective measurements and reveal a previously unreported feature of the Ham-

ming distance. Namely, for a given wave function, the minimum Hamming distance calculated with moderate sets of unique bitstrings follows a power-law scaling relative to the set size. This scaling behavior reveals the intrinsic connectivity within the state space and the corresponding power-law parameters serve as the effective descriptors of the quantum state. We show that our approach enables a simple certification of large-scale wave functions with a limited number of measurements. In turn, the analysis of the antiferromagnetic  $J_1 - J_2$  model solutions obtained with the attention-based vision transformer wave function facilitates detecting phase boundaries and estimating accuracy of the neural network approach at different points of the phase space. Furthermore, we apply our method to characterize the quench dynamics of spin-glass systems simulated on D-Wave quantum processors.

*Method.* To characterize a  $N$ -qubit quantum system that is described with a wave function  $|\Psi\rangle$  one is to perform a number of projective measurements in a basis. From these measurements we collect  $N_b^{\max}$  unique bitstrings, where the  $i$ th one is represented as  $\mathbf{x}^i = \{x_k^i\}_{k=1..N}$  and  $x_k^i = \{0, 1\}$ . Depending on the particular source of measurement data such a number can be varied from  $10^3$  for the D-Wave quantum annealer to  $10^6$  for Sycamore device. Since each sample is unique, the probabilities of individual basis states and related quantities cannot be extracted from this data. As the next step, we randomly collect  $N_b$  samples from the entire set and calculate the Hamming distances between them,  $d(\mathbf{x}^i, \mathbf{x}^j) = \sum_{k=1}^N |x_k^i - x_k^j|$ , where  $i, j = 1..N_b$  and  $i \neq j$ . For each bitstring, we determine the distance to its nearest neighbor and then average these minimum distances across the dataset of the collected  $N_b$  samples. Repeating such a procedure for different values of  $N_b$  allows us

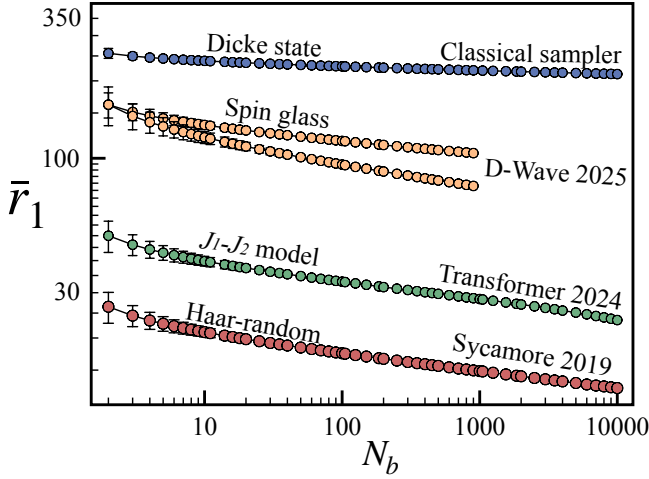


FIG. 1. Minimal Hamming distance functions calculated for a few notable quantum states (from top to bottom): the classically-sampled 512-qubit Dicke state with 256 excitations; 324-qubit spin-glass states simulated on the D-Wave quantum annealer [20] with the square lattice topology and quench times of 7 (the upper yellow curve) and 20 (the lower yellow curve) ns; ground state of the frustrated antiferromagnetic  $J_1 - J_2$  model optimized with transformer-based neural network quantum state approach [21] on  $10 \times 10$  square lattice at  $J_2 = 0.5$ ; 53-qubit Haar-random state imitated on Sycamore quantum processor [22].

to define the following function:

$$\bar{r}_1(N_b) = \frac{1}{N_b} \sum_{i=1}^{N_b} \min_{j \in \{1, \dots, N_b\}} d(\mathbf{x}^i, \mathbf{x}^j). \quad (1)$$

Usually, the average minimum distance  $\bar{r}_1$  calculated at a given  $N_b$  is to play a supporting role being used as the cutoff radius when constructing wave function networks [12, 15, 16]. Here we are going to show that the  $\bar{r}_1(N_b)$  function provides enough information for identification and discrimination of quantum states of different complexity as well as finding phase boundaries.

Figure 1 displays the  $\bar{r}_1(N_b)$  dependences in a log-log scale for several notable large-scale quantum states, for which measurement data are either publicly available from real quantum devices or can be generated on classical computers. Despite the different origin of underlying quantum data, the resulting Hamming functions calculated with measurements in the  $\sigma^z$  basis reveal similar characteristic patterns. Namely, a rapid non-linear decrease with large standard deviations at small values of  $N_b$  is replaced by almost linear behaviour with a slope specific to each wave function. This suggests to use the power-law fitting,

$$\bar{r}_1(N_b) = AN_b^{-\alpha} \quad (2)$$

for a universal representation of different quantum states, which facilitates their comparison and certification. While the coefficient  $A$  in Eq.2 corresponds to the

value of  $\bar{r}_1(N_b)$  at  $N_b = 1$ , the minimal number of bit-strings for which the Hamming distance function can be defined is two. As we will show below, the coefficient  $A$  demonstrates a great sensitivity to variations of a given quantum state, that is why we consider it as an effective quantity which is useful for certification and can be formally obtained with the  $N_b \rightarrow 1$  extrapolation of  $\bar{r}_1(N_b)$ . In turn, the exponent  $\alpha$  determines the scaling rate of finding the nearest neighbors in the state space as the sample set increases, which turns out to be extremely slow, with  $\alpha \in [0.1, 0.35]$  for the quantum states we consider in this work. Below, we provide a deeper analysis of the measurement data for the quantum state families whose representatives are shown in Fig.1.

We start with *Dicke quantum states* that can be simulated classically and generally defined as

$$|\Psi_N^D\rangle = \frac{1}{\sqrt{C_N^D}} \sum_j \mathcal{P}_j(|0\rangle^{\otimes N-D} \otimes |1\rangle^{\otimes D}). \quad (3)$$

Here  $N$  is the number of qubits,  $D$  is the parameter that controls the complexity of  $|\Psi_N^D\rangle$  through the number of “1”s in the contributing basis functions,  $C_N^D = N!/(D!(N-D)!)$  and the sum goes over all possible per-

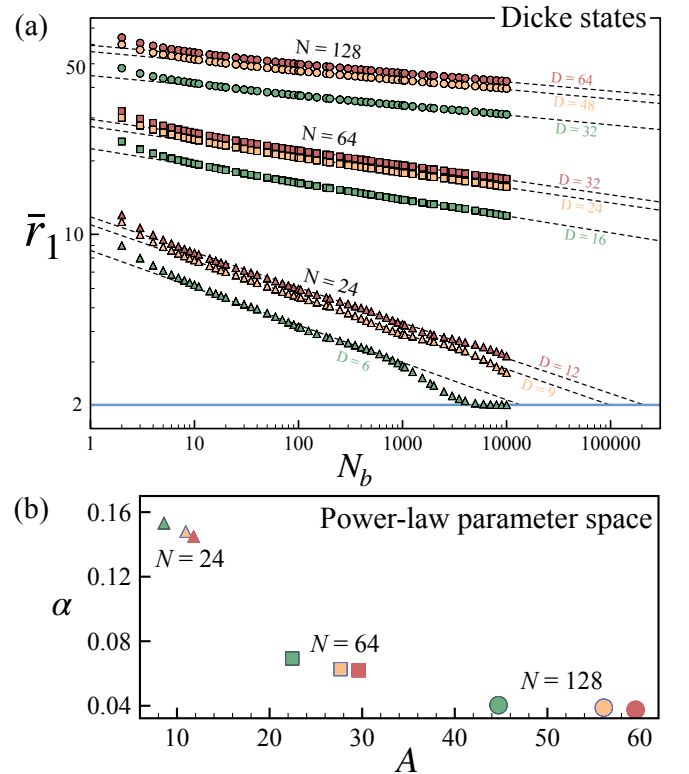


FIG. 2. (a) Average minimal distance function, Eq.1 calculated for Dicke states of 24-, 64- and 128-qubit systems in the  $\sigma^z$  basis. Each point was averaged over 10 samples. Black dashed lines denote the fit of the sampling data with Eq.2. (b) Map distinguishing the different Dicke states with respect to the power-law parameters  $A$  and  $\alpha$ .

mutations of qubits, denoted with  $\mathcal{P}_j$ . For the given  $N$  the state with  $D = N/2$  is characterized by the largest entanglement entropy [6].

Figure 2 (a) gives the  $\bar{r}_1(N_b)$  function calculated for the Dicke states of 24, 64 and 128 qubits with different number of excitations,  $D = N/2$ ,  $3N/8$  and  $N/4$ . By choosing these wave functions, we can probe different degrees of information availability when characterizing quantum states. For instance, for the 24-qubit Dicke states, a reasonable number of measurements allows to generate unique bitstrings that cover the whole Hilbert space, which is clearly not the case for the 128-qubit Dicke states. This example of the  $|\Psi_{24}^6\rangle$  with the smallest space state of 134596 gives the complete picture of functional patterns of  $\bar{r}_1$  at varying  $N_b$ . The part of the function that corresponds to  $N_b \in [10, 500]$  is well approximated with  $\bar{r}_1(N_b) = 8.59N_b^{-0.15}$ . For  $N_b > 1000$  the minimal Hamming distance is characterized by a much faster decay and saturates by the minimal value of 2 (horizontal blue line in Fig.2 (a)) at  $N_b = 5000$ .

Importantly, the larger the quantum system the more accurate approximation with the power law of the Hamming distance data. In the case of  $N = 64$  and 128 we use the range  $N_b \in [100, 10000]$  for fitting with Eq.2. From Fig.2 (b) providing power-law parameters for Dicke states one can conclude that the wave functions of the same number of qubits feature approximately the same exponent and can be distinguished by the coefficient A, which is found to be sensitive to the complexity of  $|\Psi_N^D\rangle$ . At the same time, in the case of the Dicke states  $\alpha$  is sensitive to the choice of  $N$ .

*Phase boundaries of  $J_1 - J_2$  model solutions.* The possibility of distinguishing quantum states with a limited number of measurements paves the way to a solution of phase classification problem which holds a significant importance in condensed matter physics. To demonstrate this we use a nontrivial example of the two-dimensional  $J_1 - J_2$  model with antiferromagnetic interactions between nearest ( $J_1$ ) and next-nearest ( $J_2$ ) neighbours on the  $\sqrt{N} \times \sqrt{N}$  square lattice,

$$H_{J_1-J_2} = J_1 \sum_{\langle i,j \rangle} \mathbf{S}_i \mathbf{S}_j + J_2 \sum_{\langle\langle i,j \rangle\rangle} \mathbf{S}_i \mathbf{S}_j. \quad (4)$$

Depending on the value of  $J_2$  the model is characterized by phases of different complexity. For instance, the quantum analogs of the classical Néel and stripe phases were found for  $J_2 \in [0, 0.45]$  and  $J_2 \in [0.61, 1]$ , respectively. Despite considerable efforts, there is still no consensus on the ground states of the  $J_1 - J_2$  model in the intermediate regime  $J_2 \in (0.45, 0.61)$ , which represents a special difficulty for numerical simulations [23]. To find the ground states of the  $J_1 - J_2$  model on the square lattice with periodic boundary conditions and  $N = 36, 64$  and 100 spins  $\frac{1}{2}$ , we use the exact diagonalization (ED) [24] and variational neural-network quantum state approach utilizing a Vision Transformer network (ViT) for

wave function representation [25, 26] as realized in the NetKet package [27, 28]. The details on the training and sampling procedures are provided in Appendix A.

ED results obtained for the  $J_1 - J_2$  model on the  $6 \times 6$  supercell (the red crosses in Fig.3) evidence that the power  $\alpha$  is sensitive to critical regions of the model phase diagram. In particular, it exhibits a linear behaviour for small  $J_2 \in [0, 0.3]$  and a smooth maximum spanning the known critical area ( $J_2 \in [0.5, 0.6]$ ), with the largest values attained at  $J_2 = 0.6$ . The kink observed at this point clearly signals a change in the system's state and can be attributed to the well-established boundary between intermediate and stripe phases [23]. These ED results provide a solid basis for analyzing the approximate solutions obtained with the variational ViT quantum state approach. From Fig.3 we observe an excellent agreement between ED and ViT values of the power-law parameter for  $J_2 \in [0, 0.4]$  (the Néel phase). Expectedly, the largest deviations from the exact solution takes place at the critical  $J_2 = 0.55$  and  $J_2 = 0.6$ , which agrees with

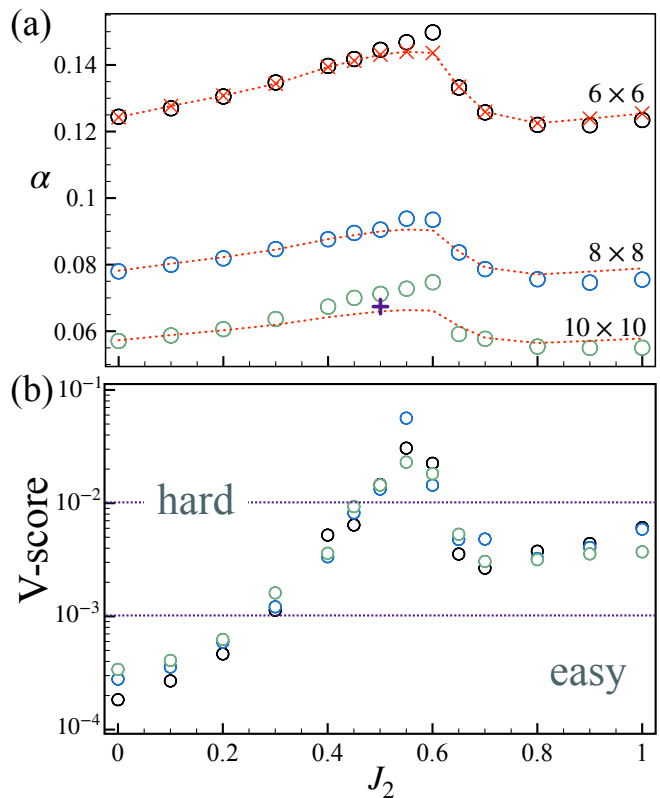


FIG. 3. (a) Power-law parameter,  $\alpha$  calculated for exact ED and approximated ViT ground states of the antiferromagnetic  $J_1 - J_2$  model. Black, blue and green circles correspond to the ViT results obtained for  $6 \times 6$ ,  $8 \times 8$  and  $10 \times 10$  supercells, respectively. Red crosses stand for ED solutions of the  $6 \times 6$  system. Red dotted lines denote ED data rescaled as described in the text. The violet plus sign corresponds to the estimate based on pre-trained ViT data from [21]. (b) V-score metric calculated for the ViT solutions with Eq.5.

largest deviations in ground state energies obtained for these points (Appendix A).

Increasing the system size leads to a suppression of the absolute values of the  $\alpha(J_2)$  function. Nevertheless, the variational profiles of the function are robust with the maximum at 0.6. To demonstrate trends more explicitly, we perform a scaling of the ED dependences obtained for the  $6 \times 6$  supercell (red dotted lines in Fig.3). For each system size, the scaling factors are defined to match the ViT data at  $J_2 = 0$ . This represents the simplest, non-frustrated regime for simulations, where reliable quantum Monte Carlo (QMC) results [29] are available. The accuracy of our ViT results at  $J_2 = 0$  can be demonstrated by calculating the relative errors of the ground state energies with respect to the QMC ones (Appendix A). Figure 3 shows that the ViT power-law parameters (green and blue circles) perfectly match the scaled  $6 \times 6$  dependences (red dotted lines) for  $J_2 \in (0, 0.3]$ . Such agreement may indicate that the ViT provides an accurate approximation of the unknown ground states in this parameter regime. In turn, outside this parameter range ( $J_2 > 0.3$ ) we observe deviations of the  $\alpha$  values from the scaled curves, which become especially pronounced for the  $10 \times 10$  system. Importantly, at  $J_2 = 0.5$  a pre-trained ViT with 434760 parameters [21] is available for  $10 \times 10$  system; this model yields a lower ground state energy and a smaller deviation of the  $\alpha$  power from the rescaled  $6 \times 6$  curve (indicated by the purple plus marker in Fig.3) in comparison with our ViT solution.

Traditionally, the system with  $J_2 = 0.5$  is considered to be the most frustrated one and is used as a benchmark point for different variational eigensolvers [21, 30]. According to our results, the largest deviations from the  $6 \times 6$  baseline are observed at  $J_2 = 0.55$  and 0.6, which suggests treating the solutions at these points to be particularly challenging for ViT-based neural quantum state approaches. To confirm these conclusions we have calculated the dimensionless V-score metric [31] that combines the variational energy,  $E$  and energy variance,  $\text{Var}E = \langle \hat{H}^2 \rangle - \langle \hat{H} \rangle^2$  estimated for an  $N$ -qubit system. For the  $J_1 - J_2$  spin model such a metric is given by

$$\text{V-score} = \frac{N \text{Var}E}{E^2}, \quad (5)$$

and is a reliable estimator for the order of magnitude of the energy relative error [31]. By using V-score, the case of the  $J_1 - J_2$  square lattice Hamiltonian was identified as a hard problem for variational algorithms where one cannot expect an energy accuracy better than one or two significant digits. Our ViT calculations presented in Fig.3 (b) confirm this for the intermediate values of  $J_2$ . In the regime of zero ( $J_2 = 0$ ) or weak ( $J_2 \in (0, 0.2]$ ) frustration, the V-score values are of the order of  $10^{-4}$ , which agrees with the previous results [31]. For all the considered systems the V-score functions feature maxima at  $J_2 = 0.55$  on the order of  $10^{-2}$ , which correlates with

the behaviour of the  $A(J_2)$  function (Appendix A). Thus, the power-law parameters enable us not only to detect phase boundaries, but also to qualitatively characterize the accuracy of the eigenvalue problem solutions.

*Intrinsic dimension of the quantum annealing data.* To demonstrate the versatility of our approach in processing data from different sources, next we analyze the samples obtained in the recent D-Wave quantum annealing experiments [20], where a quantum processing unit (QPU) is programmed to generate samples in close agreement with solutions of the Schrödinger equation for the Ising model Hamiltonian

$$H(t) = -\Gamma(t/t_a) \sum_i \sigma_i^x + \mathcal{J}(t/t_a) \sum_{ij} J_{ij} \sigma_i^z \sigma_j^z. \quad (6)$$

Here  $\sigma_i^\mu$  ( $\mu = x, z$ ) is the Pauli matrix, the couplings  $J_{ij}$  are chosen randomly with respect to the different topologies. The time-dependent coefficients  $\Gamma(t/t_a)$  and  $\mathcal{J}(t/t_a)$  control the Ising and transverse-field contributions in Eq.6 that have opposite schedules within annealing procedure ( $\Gamma(0) \gg \mathcal{J}(0)$  at  $t = 0$  and  $\Gamma(1) \ll \mathcal{J}(1)$  at the quench time  $t = t_a$ ).

A system undergoing a quantum phase transition during Schrödinger evolution is described by the quantum Kibble-Zurek mechanism [32–34], which predicts the formation of the defects due to the finite quench time,  $t_a$ . If the Ising part in Eq.6 described a spin chain with uniform ferromagnetic nearest-neighbor interactions, where the ground state corresponds to collinear ordering, the defects in the measurement results could be easily detected and characterized, as demonstrated in experiments with quantum annealers [35] and Rydberg atom platforms [36]. For the spin glasses, Eq.6 with random exchange interactions, the situation is more challenging, since the ground-truth states can be found only for small-scale systems (for instance, the  $6 \times 6$  square lattice). Fortunately,

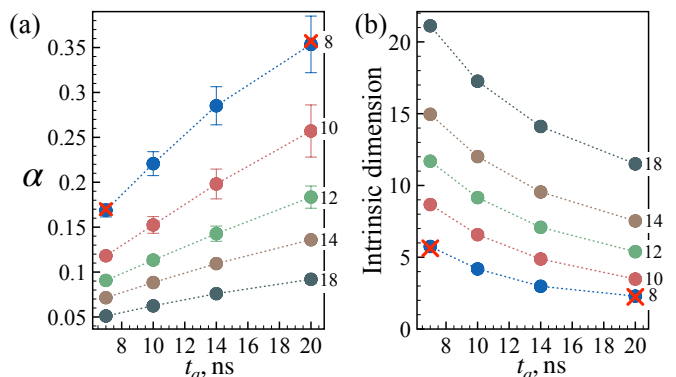


FIG. 4. (a) Dependence of the power  $\alpha$  on the annealing time calculated for D-Wave sampling data [20]. Numbers on the right indicate linear system sizes. These results were averaged over 20 instances. (b) Intrinsic dimension averaged over 20 instances. Red crosses denote the power  $\alpha$  (a) and ID (b) calculated for MPS  $8 \times 8$  samples from Ref.20.

the spin-glass order parameter  $\langle q^2 \rangle$  [37] allows quantifying the degree of spin-freezing. Its increase toward unity signifies a reduction in the number of defects and a closer approach to the ideal spin-glass configuration.

In turn, our approach facilitates a better understanding of the state-space structure and its evolution with  $t_a$ . Specifically, we analyze experimental data [20] for a system with a square lattice topology, as it provides the largest available set of bitstrings. The  $\bar{r}_1(N_b)$  functions calculated for the  $18 \times 18$  system at different quench times [Fig.1] show a clear trend toward faster decay as  $N_b$  increases. Such a tendency can be quantified with the  $\alpha$  parameter from the power-law fitting of  $\bar{r}_1(N_b)$  and persists for smaller models [Fig.4 (a)]. This indicates that the longer quench time leads to stronger localization of the system's wave function in the state space.

Next, to determine the minimum number of degrees of freedom necessary to represent the information content of the experimental data, the intrinsic dimension (ID) is employed. To estimate this quantity, we use the two nearest neighbors estimator [38], which performs well under the assumption that the data density is locally constant. The detailed description of this measure is given in the Appendix B. Despite the D-Wave data are presented by N-dimensional vectors, the calculated ID evidence on a redundancy of such a representation. For instance, at  $t_a = 7$  ns the intrinsic dimension is the order of the linear system size,  $ID \sim \sqrt{N}$  [Fig.4 (b)]. The obtained results show that ID further decreases with  $t_a$ , which means that the dimensionality of the subspace containing the basis states of the system's wave function is becoming smaller.

The quench dynamics of small-size spin-glass systems can be accurately reproduced with classical approaches such as the matrix product state (MPS) [20]. We likewise observe excellent agreement between MPS and QPU Hamming-distance quantities characterizing state space [Fig.4] of system with the  $8 \times 8$  square lattice. Simulations of larger systems with the same or more complex topologies represent a significant challenge for classical methods. Here, information on state-space properties extracted from experimental data could prove useful for further optimization of classical algorithms. For instance, our results demonstrate a simplification of the wave-function structure with  $t_a$ , which motivates the search for more effective classical representations of quantum wave functions with fewer parameters similar to the static case [39–43].

*Conclusions.* To sum up, we have revealed a common feature of quantum data obtained from different sources, which is the power-law behavior of the minimal Hamming distance with the number of samples. This universality enables the extraction of quantum state characteristics, such as power-law parameters, independently of the sample size. On this basis, we have explored a number of important problems in quantum computing and condensed matter physics including the certification

of quantum states, the accuracy of neural quantum state solutions, and state space analysis of quantum annealing experiments. The introduced Hamming-distance parameters provide information on connectivity in the state space and thus complement problem-specific quantities, such as order parameters.

## ACKNOWLEDGEMENTS

We would like to thank Oleg Sotnikov for technical assistance. This work was supported by the Russian Science Foundation, Grant No. 26-12-00377, <https://rscf.ru/project/26-12-00377/>.

## APPENDIX A

### Calculation details

In this section we present technical details concerning calculations of the  $J_1 - J_2$  models and compare our results with previous works. For small-size systems (36 spins) we use exact diagonalization approach as realized in SpinED package [24]. In turn, for larger systems one needs to employ an approximate scheme, such as variational neural quantum state (NQS) approach. We use the NetKet package realization [27, 28] of an attention-based vision transformer wave function [25, 26], as it is one of the most promising architectures for solving large-scale frustrated magnetic models [44]. For all the system's sizes we use the same number of the training epochs (1500) and the same ViT architecture that comprises 4 layers, 12 attention heads and embedding dimension of 60, which results in  $\sim 1.5 \times 10^5$  trainable parameters. To update the network parameters we use stochastic reconfiguration approach [21] with the built-in `MetropolisExchange` sampling method. The corresponding number of samples is 4096.

Tables I gives the ground state energies obtained for  $J_1 - J_2$  Hamiltonian defined on supercells of different sizes. In the case of the  $6 \times 6$  supercell we compare the ViT energies with the exact diagonalization results. The latter are in full agreement with previous works [45]. The largest deviations between ViT and ED results take place for critical values of  $J_2$  from 0.5 to 0.6. At the same time the best agreement is observed for the Néel phase. As an important benchmark for our non-frustrated results obtained at  $J_2 = 0$  we consider the Quantum Monte Carlo (QMC) method which provides accurate ground state energies for large-scale systems (up to  $96 \times 96$  spins in [29]). The relative errors of the ViT ground state energies with respect to the QMC ones are approximately equal to  $3 \times 10^{-4} \%$  ( $6 \times 6$  supercell),  $8 \times 10^{-3} \%$  ( $8 \times 8$ ) and  $1 \times 10^{-2} \%$  ( $10 \times 10$ ). For the systems on the  $8 \times 8$

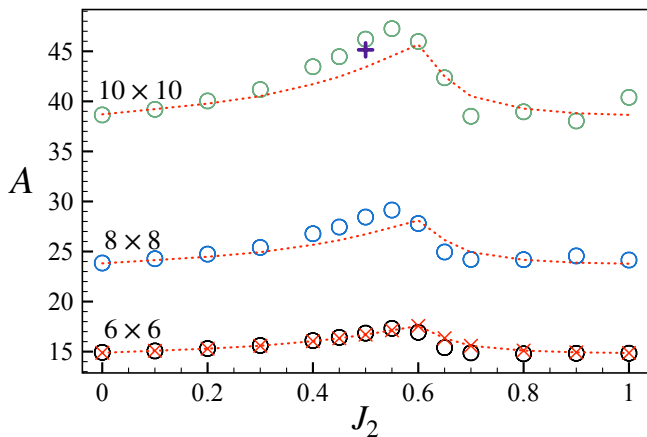


FIG. 5. Power-law parameter,  $A$  calculated for exact ED and approximated ViT ground states of the antiferromagnetic  $J_1 - J_2$  model. Black, blue and green circles correspond to the ViT results obtained after 1500 training epochs for  $6 \times 6$ ,  $8 \times 8$  and  $10 \times 10$  supercells, respectively. Red crosses stand for exact diagonalization solutions of the  $6 \times 6$  system. Red dotted lines denote ED data rescaled as described in the main text. The violet plus sign corresponds to the estimate based on pre-trained ViT data from [21].

and  $10 \times 10$  supercells simulated by using  $J_2 > 0$  we compare our ViT estimations of the ground state energy with best results (the lowest energies) available in the literature. From Table I one can see that for some values of  $J_2$  we obtain a lower energy than known estimates.

*Minimal Hamming-distance function.* To construct the  $\bar{r}_1(N_b)$  function by using the set of the  $N_b^{max}$  unique samples we used the following procedure. (i) For each value of  $N_b$  we randomly choose  $N_b$  bitstrings from the set of available  $N_b^{max}$  samples. (ii) Then, for each bitstring one finds the minimal Hamming distance,  $r_1$  to other  $N_b - 1$  samples. (iii) The minimal distances are averaged over chosen  $N_b$  bitstrings.

This procedure is repeated several times and the resulting  $\bar{r}_1$  values are averaged. As shown in Fig.1, this gives finite dispersion for small values of  $N_b$  ranging from 2 to 10. Importantly, the  $\bar{r}_1$  function is defined for  $N_b < N_b^{max}$ . For instance, in the case of the D-Wave data,  $N_b^{max}$  does not exceed 1000, so we use  $N_b$  between 700 and 900, depending on the number of available unique bitstrings.

Figure 5 complements Fig.3 presented in the main text and gives the  $A$  parameters from the power-law fitting (Eq.2) of the  $\bar{r}_1(N_b)$  functions calculated for the  $J_1 - J_2$  model of different sizes. The ViT results denoted with color circles features maximum at 0.55, which agrees with the V-score metric.

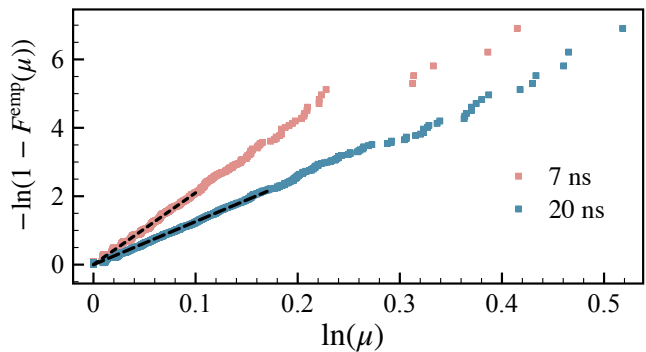


FIG. 6. Example of cumulative distributions against  $\mu$  obtained for one specific disorder realization for the  $18 \times 18$  D-Wave data at  $t_a = 7$  ns and  $t_a = 20$  ns. The corresponding ID values defined from fit are equal to 21 and 12.59, respectively.

## APPENDIX B

The initial dimension of the feature-vectors describing the system in question is usually excessive and the data can be embedded in lower-dimensional space. The dimensionality of such a subspace is called an Intrinsic Dimension (ID) [49] and can be associated with the minimal amount of the degrees of freedom and, therefore, with Kolmogorov complexity [50].

In the two nearest neighbors estimator method [38], the intrinsic dimension is defined with the following equation

$$\text{ID} = -\frac{\ln[1 - F^{\text{emu}}(\mu)]}{\ln(\mu)}, \quad (7)$$

where  $F^{\text{emu}}(\mu)$  is the empirical cumulative distribution function and  $\mu = r_2/r_1$  is calculated for each bitstring, where  $r_1$  and  $r_2 \geq r_1$  are the Hamming distances to the nearest and next-nearest neighbours, respectively.

To calculate the ID of the dataset including  $N_b$  bitstrings one needs to sort  $\mu$  values in the ascending order. After doing this, the empirical cumulative distribution function corresponding to  $i$ th bitstring in the sorted dataset can be defined as  $F^{\text{emu}}(\mu_i) = \frac{i}{N_b}$ . Thus, the resulting points will have coordinates  $\{-\ln[1 - F^{\text{emu}}(\mu_i)], \ln(\mu_i) | i = 1, \dots, N_b\}$  and should be fitted with the straight line passing through the origin. The intrinsic dimension is simply the slope of this line (Fig. 6). To make the procedure more robust, we discard the 10% of the points characterized by highest values of  $\mu$  from the fitting as it was proposed in [38].

The ID can be utilized to assess the complexity of quantum states [12] and is useful to find the most appropriate basis in which one should perform measurements to analyze the specific quantum system [16]. In some cases assessing the intrinsic dimension in different bases even helps to detect the phase transition in quantum models. In these respect, the ID is closely related

TABLE I. Ground state energies of the  $J_1 - J_2$  model obtained in this work with exact diagonalization (ED) and variational NQS approach utilizing vision transformer wave function (ViT). The comparison with the best results of previous works is also given.

$J_2$	$J_1 - J_2$ model					
	$6 \times 6$ , ED (this work)	$6 \times 6$ , ViT (this work)	$8 \times 8$ , ViT (this work)	$8 \times 8$ (previous works)	$10 \times 10$ , ViT (this work)	$10 \times 10$ (previous works)
0.00	-0.678872	-0.678870	-0.673434	-0.67349005 [29]	-0.671476	-0.67155266[29]
0.10	-0.638095	-0.638078	-0.633093		-0.631365	-
0.20	-0.599046	-0.599044	-0.594508		-0.592982	-0.592847 [48]
0.30	-0.562459	-0.562453	-0.558295		-0.556912	-
0.40	-0.529744	-0.529547	-0.525513	-0.525492 [23]	-0.524361	-0.5240 [46]
0.45	-0.515658	-0.515281	-0.510970	-0.511117 [23]	-0.509661	-0.51001 [46]
0.50	-0.503809	-0.502970	-0.498115	-0.498460 [23]	-0.496783	-0.4976921 [30]
0.55	-0.495177	-0.493676	-0.483143	-0.48781 [23]	-0.485759	-0.48693 [46]
0.60	-0.493238	-0.490755	-0.481606		-0.477623	-0.47839 [47]
0.65	-0.506590	-0.506299	-0.498312		-0.494672	-
0.70	-0.529989	-0.529884	-0.522091		-0.519035	-0.51889 [48]
0.80	-0.586485	-0.585780	-0.577310		-0.574130	-0.57404 [48]
0.90	-0.649048	-0.647371	-0.637518		-0.634170	-
1.00	-0.714356	-0.712413	-0.700508		-0.696641	-0.69670 [48]

with the dissimilarity measure proposed recently by some of us [6]. This quantity was designed to detect phase transitions in quantum systems and is based on the analysis of the complexity of patterns presented in data.

- 
- [1] J.Y. Khoo and M. Heyl, Quantum entanglement recognition. *Phys. Rev. Res.* 3, 033135 (2021).
- [2] S. Aaronson, Shadow tomography of quantum states. *SIAM J. Comput.* 49, STOC18-368-STOC18-394 (2020).
- [3] H.-Y. Huang, R. Kueng, and J. Preskill, Predicting many properties of a quantum system from very few measurements. *Nat. Phys.* 16, 1050–1057 (2020).
- [4] D. A. Konyshov and V. V. Mazurenko, Estimating classical mutual information between quantum subsystems with neural networks, *Phys. Rev. E* 113, 034122 (2026).
- [5] Z. Goldfeld, D. Patel, S. Sreeksumar, and M. M. Wilde, Quantum neural estimation of entropies, *Phys. Rev. A* 109, 032431 (2024).
- [6] O. M. Sotnikov et al., Certification of quantum states with hidden structure of their bitstrings, *npj Quantum Inf.* 8, 41 (2022).
- [7] A. A. Bagrov, I. A. Iakovlev, A. A. Iliasov, M. I. Katsnelson, and V. V. Mazurenko, Multiscale structural complexity of natural patterns, *Proc. Natl. Acad. Sci. USA* 117, 30241 (2020).
- [8] Oleg M. Sotnikov, Ilia A. Iakovlev, Evgeniy O. Kiktenko, Aleksey K. Fedorov, and Vladimir V. Mazurenko, Achieving the volume-law entropy regime with random-sign Dicke states, *Phys. Rev. A* 110, 062416 (2024).
- [9] B. Xiao, J. R. Moreno, M. Fishman, D. Sels, E. Khatami, and R. Scalettar, Extracting off-diagonal order from diagonal basis measurements, *Phys. Rev. Res.* 6, L022064 (2024).
- [10] E. Ibarra-García-Padilla, S. Striegel, R. T. Scalettar, and E. Khatami, Structural complexity of snapshots of two-dimensional Fermi-Hubbard systems, *Phys. Rev. A* 109, 053304 (2024).
- [11] R. W. Hamming, Error Detecting and Error Correcting Codes, *Bell System Technical Journal* 29, 147 (1950).
- [12] T. Mendes-Santos, M. Schmitt, A. Angelone, A. Rodriguez, P. Scholl, H. J. Williams, D. Barredo, T. Lahaye, A. Browaeys, M. Heyl, and M. Dalmonte, Wave-function network description and Kolmogorov complexity of quantum many-body systems, *Phys. Rev. X* 14, 021029 (2024)
- [13] I. A. Iakovlev, O. M. Sotnikov, I. V. Dyakonov, E. O. Kiktenko, A. K. Fedorov, S. S. Straupe, and V. V. Mazurenko, Benchmarking a boson sampler with Hamming nets, *Phys. Rev. A* 108, 062420 (2023).
- [14] A. A. Mazanik, A. N. Rubtsov, Boson sampling validation approach by examining the sample space filling, *Phys. Rev. A* 112, 012619 (2025).
- [15] Laurin Brunner, Tobias Wiener, Tiago Mendes-Santos, Reyhaneh Khasseh, and Markus Heyl, Snapshot renormalization group for quantum matter, arXiv:2510.12415.
- [16] Riccardo Andreoni, Vittorio Vitale, Cristiano Muzzi, Guido Caldarelli, Roberto Verdel, and Marcello Dalmonte, Network theory classification of quantum matter based on wave function snapshots, arXiv:2512.02121.
- [17] K. J. Satzinger et al., Realizing topologically ordered states on a quantum processor, *Science* 374, 1237-1241 (2021).
- [18] M. Ippoliti, K. Kechedzhi, R. Moessner, S. L. Sondhi, and V. Khemani, Many-body physics in the NISQ era: Quantum programming a discrete time crystal, *PRX Quant.* 2, 030346 (2021).
- [19] E. A. Maletskii, I. A. Iakovlev, and V. V. Mazurenko, Quantifying spatiotemporal patterns in classical and quantum systems out of equilibrium, *Phys. Rev. E* 109, 024105 (2024)
- [20] A.D. King et al., Beyond-classical computation in quantum simulation, *Science* 388, 199-204 (2025).
- [21] Riccardo Rende, Luciano Loris Viteritti, Lorenzo Bar-

- done, Federico Becca, Sebastian Goldt, A simple linear algebra identity to optimize large-scale neural network quantum states, *Communications Physics* 7, 260 (2024)
- [22] F. Arute, et al. Quantum supremacy using a programmable superconducting processor. *Nature* 574, 505–510 (2019).
- [23] Yusuke Nomura, Masatoshi Imada, Dirac-type nodal spin liquid revealed by refined quantum many-body solver using neural-network wave function, correlation ratio, and level spectroscopy, *Phys. Rev. X* 11, 031034 (2021).
- [24] T. Westerhout, Lattice-symmetries: A package for working with quantum many-body bases, *J. Open Source Softw.* 6, 3537 (2021).
- [25] Luciano Loris Viteritti, Riccardo Rende, and Federico Becca, Transformer variational wave functions for frustrated quantum spin systems, *Physical Review Letters* 130, 236401 (2023).
- [26] Luciano Loris Viteritti, Riccardo Rende, Alberto Parola, Sebastian Goldt, and Federico Becca, Transformer wave function for two dimensional frustrated magnets: Emergence of a spin-liquid phase in the Shastry-Sutherland model, *Phys. Rev. B* 111, 134411 (2025).
- [27] Giuseppe Carleo, Kenny Choo, Damian Hofmann, James E. T. Smith, Tom Westerhout, Fabien Alet, Emily J. Davis, Stavros Efthymiou, Ivan Glasser, Sheng-Hsuan Lin, Marta Mauri, Guglielmo Mazzola, Christian B. Mendl, Evert van Nieuwenburg, Ossian O’Reilly, Hugo Théveniaut, Giacomo Torlai, Alexander Wietek, NetKet: A Machine Learning Toolkit for Many-Body Quantum Systems, *SoftwareX* 10, 100311 (2019).
- [28] Filippo Vicentini, Damian Hofmann, Attila Szabó, Dian Wu, Christopher Roth, Clemens Giuliani, Gabriel Pescia, Jannes Nys, Vladimir Vargas-Calderon, Nikita Astrakhantsev, Giuseppe Carleo, NetKet 3: Machine Learning Toolbox for Many-Body Quantum Systems, *SciPost Phys. Codebases* 7 (2022).
- [29] Anders W. Sandvik, High-precision ground state parameters of the two-dimensional spin-1/2 Heisenberg model on the square lattice, *J. Stat. Mech.* 043101 (2026).
- [30] Ao Chen and Markus Heyl, Empowering deep neural quantum states through efficient optimization, *Nature Physics* 20, 1476 (2024).
- [31] Dian Wu, Riccardo Rossi, Filippo Vicentini, Nikita Astrakhantsev, Federico Becca, Xiaodong Cao, Juan Carrasquilla, Francesco Ferrari, Antoine Georges, Mohamed Hibat-Allah, Masatoshi Imada, Andreas M. Läuchli, Guglielmo Mazzola, Antonio Mezzacapo, Andrew Millis, Javier Robledo Moreno, Titus Neupert, Yusuke Nomura, Jannes Nys, Olivier Parcollet, Rico Pohle, Imelda Romero, Michael Schmid, J. Maxwell Silvester, Sandro Sorella, Luca F. Tocchio, Lei Wang, Steven R. White, Alexander Wietek, Qi Yang, Yiqi Yang, Shiwei Zhang, Giuseppe Carleo, Variational benchmarks for quantum many-body problems, *Science* 386, 296–301 (2024).
- [32] A. Polkovnikov, Universal adiabatic dynamics in the vicinity of a quantum critical point, *Phys. Rev. B* 72, 161201 (2005).
- [33] W. H. Zurek, U. Dorner and P. Zoller, Dynamics of a quantum phase transition, *Physical Review Letters* 95(10), 105701 (2005).
- [34] J. Dziarmaga, Dynamics of quantum phase transition: exact solution in quantum Ising model, *Phys. Rev. Lett.* 95, 245701 (2005).
- [35] Andrew D. King, Sei Suzuki, Jack Raymond, Alex Zucca, Trevor Lanting, Fabio Altomare, Andrew J. Berkley, Sara Ejtemaee, Emile Hoskinson, Shuiyuan Huang, Eric Ladizinsky, Allison MacDonald, Gaelen Marsden, Travis Oh, Gabriel Poulin-Lamarre, Mauricio Reis, Chris Rich, Yuki Sato, Jed D. Whittaker, Jason Yao, Richard Harris, Daniel A. Lidar, Hidetoshi Nishimori, and Mohammad H. Amin, Coherent quantum annealing in a programmable 2000-qubit Ising chain, *Nature Physics* 18, 1324–1328 (2022).
- [36] Alexander Keesling, Ahmed Omran, Harry Levine, Hannes Bernien, Hannes Pichler, Soonwon Choi, Rhine Samajdar, Sylvain Schwartz, Pietro Silvi, Subir Sachdev, Peter Zoller, Manuel Endres, Markus Greiner, Vladan Vuletić, and Mikhail D. Lukin, Quantum Kibble-Zurek mechanism and critical dynamics on a programmable Rydberg simulator, *Nature* 568, 207 (2019).
- [37] S.F. Edwards and P.W. Anderson, Theory of spin glasses, *J. Phys. F: Met. Phys.* 5, 965 (1975).
- [38] E. Facco, M. d’Errico, A. Rodriguez, and A. Laio, Estimating the intrinsic dimension of datasets by a minimal neighborhood information, *Scientific reports* 7, 12140 (2017).
- [39] Oleg M. Sotnikov, Ilia A. Iakovlev, Evgeniy O. Kiktenko, Mikhail I. Katsnelson, Aleksey K. Fedorov and Vladimir V. Mazurenko, Emergence of global receptive fields capturing multipartite quantum correlations, *Phys. Rev. B* 112, 054425 (2025).
- [40] D. Perez-Garcia, F. Verstraete, M. M. Wolf, and J. I. Cirac, Matrix product state representations, *Quantum Inf. Comput.* 7, 401 (2007).
- [41] M. Y. Pei and S. R. Clark, Compact neural-network quantum state representations of Jastrow and stabilizer states, *J. Phys. A: Math. Theor.* 54, 405304 (2021).
- [42] G. Carleo, Y. Nomura, and M. Imada, Constructing exact representations of quantum many-body systems with deep neural networks, *Nat. Commun.* 9, 5322 (2018).
- [43] X. Gao and L.-M. Duan, Efficient representation of quantum many-body states with deep neural networks, *Nat. Commun.* 8, 662 (2017).
- [44] Luciano Loris Viteritti, Riccardo Rende, Subir Sachdev, Giuseppe Carleo, Approaching the Thermodynamic Limit with Neural-Network Quantum States, arXiv:2602.02665.
- [45] H. J. Schulz, T. A. L. Ziman, D. Poilblanc, Magnetic order and disorder in the frustrated quantum Heisenberg antiferromagnet in two dimensions, *J. Physique I*, 6, 675 (1996).
- [46] W.-J. Hu, F. Becca, A. Parola, and S. Sorella, Direct evidence for a gapless Z2 spin liquid by frustrating Néel antiferromagnetism. *Phys. Rev. B* 88, 060402 (2013).
- [47] Xiao Liang, Mingfan Li, Qian Xiao, Junshi Chen, Chao Yang, Hong An, and Lixin He, Deep learning representations for quantum many-body systems on heterogeneous hardware, *Mach. Learn.: Sci. Technol.* 4, 015035 (2023).
- [48] H. Chen, D. Hendry, P. Weinberg, and A. Feiguin, Systematic improvement of neural network quantum states using Lanczos. in *Advances in Neural Information Processing Systems Vol. 35* (eds. Koyejo, S. et al.) 7490–7503 (Curran Associates, Inc., 2022).
- [49] P. Campadelli, E. Casiraghi, C. Ceruti, A. Rozza, The Physical Implementation of Quantum Computation, *Progr. Phys. Fortschr. Phys.* 48, 771–783 (2000).
- [50] A. N. Kolmogorov, On tables of random numbers, *Sankhya A* 4, 369 (1963).